Reac Kinet Mech Cat (2016) 119:595–613
DOI 10.1007/s11144-016-1080-z

Characteristics and catalytic behavior of NiAlCe catalysts in the hydrogenation of canola oil: the effect of cerium on *cis/trans* selectivity

Marcin Konkol[1] · Robert Bicki[1] · Małgorzata Kondracka[1] · Katarzyna Antoniak-Jurak[1] · Paweł Wiercioch[1] · Wiesław Próchniak[1]

Received: 21 June 2016 / Accepted: 31 August 2016 / Published online: 13 September 2016

Abstract A series of co-precipitated cerium-promoted nickel–aluminum catalysts was prepared. The physicochemical properties of the precursors were analyzed by means of various methods including XRF, HT-XRD, TPR, surface area and thermal decomposition as well as porosity measurements. The activity and selectivity of the NiAlCe catalysts in the hydrogenation reaction of canola oil were investigated and the results compared to those for the cerium-free catalyst. Besides improving some physicochemical properties of the precursors, the addition of cerium significantly improved the *cis/trans* selectivity, yet at the expense of some loss of the activity in case of larger cerium loadings. Upon addition of a relatively low amount of cerium (0.67 wt%) the content of the C18:1 *trans* fraction decreased by ca. 35 %. Together with the synergistic effect of the hydrogen pressure a significant decrease of the C18:1 *trans* fraction by ca. 48 % could be achieved. Furthermore, compared to the cerium-free catalyst, the addition of cerium resulted in a slower drop of the C18:1 *cis* fraction and a slower increase of the C18:0 fraction in time during the hydrogenation process.

Keywords Nickel catalyst · Cerium · Hydrogenation · Canola oil · *Cis/trans* selectivity · Fatty acids

Introduction

In industrial practice, the hydrogenation of vegetable oils is most often carried out on nickel catalysts [1, 2]. The main disadvantage of nickel catalysts is the necessity to perform the process at higher temperatures (>150 °C) at which adverse *cis/trans*

✉ Marcin Konkol
marcin.konkol@ins.pulawy.pl

[1] New Chemical Syntheses Institute, Al. Tysiąclecia Państwa Polskiego 13A, 24-110 Puławy, Poland

isomerization is favored. The content of TFA isomers (*trans fatty acids*) in vegetable oils hydrogenated on nickel catalysts reaches up to 40–50 %, whereas the content of positional isomers can be in the range of 30–60 % [3]. *Trans* isomers of fatty acids have higher melting points than *cis* forms. Therefore, from the process viewpoint isomerization to *trans* forms is desirable, since a moderate growth of the melting point of oil is achieved at lower degree of hydrogenation, which translates into lower hydrogen consumption and therefore lower costs. However, this process is very unfavorable from a medical point of view. Research findings show that TFAs formed during hydrogenation are deposited on the walls of blood vessels, eventually leading to their obstruction and consequently increasing the risk of coronary heart disease [4, 5]. Moreover, TFAs reduce the level of high density cholesterol fraction ("good cholesterol", HDL) and increase the level of low density cholesterol fraction ("bad cholesterol", LDL) [6, 7]. Studies on the consumption of fats in food carried out by Mozaffarian et al. suggest even a four to fivefold increase in the risk of coronary heart disease when saturated fats are replaced with *trans* unsaturated fats [8].

The adverse effects of TFA isomers generated during conventional hydrogenation on nickel catalysts have triggered research on new type of catalysts (e.g., zeolites, precious metals) [3, 9–12], novel process solutions (e.g., electrocatalytic hydrogenation, hydrogenation in liquids under supercritical conditions) [13] and modifications of fat components by interesterification, fractionation or blending [14]. Despite an intensive development of alternative methods to obtain semi-solid and solid fatty components, which do not contain TFAs and have the desired melting point and physicochemical properties, conventional hydrogenation remains an easier and often less expensive method to obtain components with defined properties that are used for the manufacture of fatty products e.g., margarines and confectionery fats. Apart from the genetic modifications of edible oils that enable to obtain oils with a large proportion of monounsaturated fatty acids, "shallow" hydrogenation through partial saturation of double bonds is the only means to increase thermal and oxidative stability of many highly unsaturated edible oils (e.g., soybean, sunflower, canola).

However, a necessary condition imposed now on the process of partial hydrogenation of vegetable oils is to eliminate the formation of *trans* fatty acids, while maintaining desired physical properties and stability of hydrogenated fat components. This limitation of *trans* isomers should ideally go hand in hand with as small as possible increase in the proportion of saturated fatty acids, mainly stearic acid, whose presence affects taste of the product ("sand taste"). Therefore, the oil industry is still looking for new selective hydrogenation catalysts or modifications of this process that could enable to obtain partially hydrogenated products free of *trans* isomers, while simultaneously maintaining appropriate content of saturated fatty acids. Additionally, the process should be characterized by low investment costs and it should remain relatively cost-effective, which in the case of many proposed methods for reducing the amount of *trans* isomers would be problematic or difficult to accomplish. For these reasons, despite many efforts of researchers, the elimination of *trans* isomers remains one of the main challenges of the oil industry and is still a subject of ongoing research.

Cerium oxide and cerium-promoted catalysts have been reported to exhibit catalytic activity and improve the selectivity in hydrogenation of various organic substrates [15–17] as well as carbon oxides [18–22]. However, in the literature data, there are hardly any reports on the activity of cerium compounds in hydrogenation reactions of oils and fats. To the best of our knowledge the only report by Alouche et al. concerns only "shallow" hydrogenation with a change of iodine value (IV) of 7–10 units [23]. During such mild hydrogenation the *trans* isomers are formed to much lesser extent.

The subject of our studies is the investigation of the physicochemical properties of cerium-promoted nickel–aluminum precursors and catalysts, their catalytic activity and selectivity in the deeper hydrogenation reaction of canola oil to the iodine value of ca. 70 (ΔIV = ca. 45) at a wide range of hydrogen pressures. Such depth of hydrogenation corresponds to that in the production of fatty acid components for margarine and shortenings on an industrial scale.

Experimental

Materials and synthesis

As feedstock, a refined, bleached, low-erucic acid canola oil was used. The nickel catalysts were prepared from the corresponding NiAlCe precursors obtained by means of co-precipitation. The precursor is chemically a mixture of nickel–aluminum hydroxycarbonates with a general formula: $Ni_mAl_n(CO_3)_x(OH)_y{\cdot}zH_2O$. The co-precipitation was carried out in a continuous mode from aqueous solutions of nickel and cerium nitrates and an aqueous solution of sodium aluminate using a Na_2CO_3/NaOH mixture with a molar ratio 2:1 as a precipitating agent. The appropriate concentrations of reagents were chosen so that the desired stoichiometry of precursors was ensured. The co-precipitation was carried out in a reaction vessel (HWS), maintaining pH of the suspension in the range 7–7.4 and temperature of 80 ± 5 °C. The precipitates were then filtered and washed until filter conductivity below 100 μS was reached. The resulting precursors were dried at 105 °C for 12 h. They are denoted as NiAl_0Ce, NiAl_1Ce, NiAl_2Ce and NiAl_3Ce according to the increasing cerium content. The precursors were concurrently calcined and reduced with hydrogen at the temperature of 450 °C for 2 h and at 550 °C for additional 2 h followed by coating of the resulting pyrophoric material at ambient atmosphere in fully hydrogenated vegetable fat. The catalysts were finally formed into pellets. They are denoted as NiAl_0Ce_C, NiAl_1Ce_C, NiAl_2Ce_C and NiAl_3Ce_C throughout this publication.

Characterization

The chemical composition of precursors was determined by means of the WDXRF method using a Panalytical Axios spectrometer. The XRD measurements of precursors were performed on a PANalytical Empyrean system (Bragg–Brentano geometry) equipped with a PIXcel^{3D} detector, using Cu K_α radiation (λ = 1.542 Å)

and operating at 40 kV and 40 mA. The X-ray diffraction patterns were refined with a sum of pseudo-Voigt profile functions and an appropriate background function using a Highscore Plus software. Temperature-programmed XRD measurements were carried out in an Anton Paar HTK-16N chamber. A sample was deposited as a thin layer (ca. 0.2–0.4 mm) on a Pt heating strip. A Pt/10 %-RhPt thermocouple spot-welded to the bottom of the heating strip was used for measuring the temperature. The decomposition/reduction process of the NiAlCe precursors was carried out in situ using 5 % H_2 in N_2 as a reducing agent (flow rate 75 ml/min). The in situ XRD patterns of the samples were recorded after their isothermal treatment for 15 min at each temperature.

The nickel content in the catalysts was analyzed by means of the gravimetric method with dimethylglyoxime, whereas the cerium content was analyzed by means of the emission atomic spectroscopy method with inductively coupled plasma (ICP-OES). The analysis was carried out on a Varian 720-ES ICP-OES spectrometer with vertically oriented, radially viewed plasma.

The thermal decomposition studies of precursors were carried out using a Netzsch STA 449 Jupiter thermal analyzer coupled with a QMS 430C Aëolos mass spectrometer. The measurements were performed in a synthetic air stream by means of TG-DSC, elevating the sample temperature with a rate of 10 °C/min. The changes of the sample weight and *m/z* signals corresponding to H_2O and CO_2 were constantly monitored during the measurement.

The specific surface area of the samples was determined by means of the nitrogen adsorption method at the temperature of liquid nitrogen (−196 °C) using a Micromeritics ASAP 2050 analyzer. The BET isotherms were measured in the p/p_0 range 0.05–0.3. The pore volume and pore size distribution (in the pore size range from 2 to 300 nm) were determined from N_2 adsorption isotherm in the $p/p_0 = 0.02–0.99$ using the BJH method.

The TPR measurements were performed using a Micromeritics AutoChem 2950HP system. A precursor sample (ca. 30 mg) was placed in a quartz U-shape microreactor and heated in a stream of 5 % H_2/Ar (40 ml/min) increasing the temperature with a rate 10 °C/min. The water vapor formed was frozen out with dry ice. The changes of hydrogen concentration were monitored by means of a TCD detector.

The nickel surface area (S_{Ni}) was determined via oxygen chemisorption at the temperature of 0 °C using a Micromeritics AutoChem 2950HP analyzer and according to the reaction: $2Ni + O_2 \rightarrow 2NiO$. Before the measurement, a sample was reduced with hydrogen at 500 °C for 2 h. The nickel surface area, dispersion and average nickel crystallite size parameters were calculated from the following Eqs. 1–4:

$$S_{Ni\_A} = \frac{n_m \cdot x_{Ni} \cdot N_A \cdot A_V}{m_p} \quad (1)$$

In this equation, the following notations are used: S_{Ni_A}—nickel surface area per 1 g of catalyst (m^2/g_{cat}), n_m—number of moles of a gas-adsorbate used during a measurement (mol), x_{Ni}—number of moles of a metal corresponding to 1 mol of the

gas-adsorbate under the measurement conditions (1.1765 mol Ni/mol O_2), N_A—nickel atom area (m^2) (N_A for Ni = 6.45 × 10^{-20} m^2), A_V—Avogadro number (6.023 × 10^{23} at/mol), m_p—sample weight (g)

$$S_{Ni\_B} = \frac{n_m \cdot x_{Ni} \cdot N_A \cdot A_V \cdot 100}{\%_{Ni} \cdot m_p} \tag{2}$$

In this equation, the following notations are used: S_{Ni_B}—nickel surface area per 1 g of nickel (m^2/g_{Ni}), $\%_{Ni}$—nickel content in a sample (%)

$$D = \frac{n_m \cdot x_{Ni} \cdot M_{Ni} \cdot 10^4}{\%_{Ni} \cdot m_p} \tag{3}$$

In this equation, the following notations are used: D—nickel dispersion (%), M_{Ni}—molar mass of nickel (g/mol)

$$d = \frac{6}{S_{Ni} \cdot g_{Ni}} \tag{4}$$

The following notations are used: d—average nickel crystallite size (spherical particle shape) (nm), g_{Ni}—nickel density (kg/dm^3).

Hydrogenation tests

The hydrogenation reactions were carried out using a high pressure installation consisting of (a) pressure autoclave Parr 5500, (b) pressure, temperature and stirring speed controller, (c) hydrogen reservoir (volume 1.0 × 10^{-4} m^3) and (d) digital manometer with an accuracy up to 0.1 bar. The tests were performed under the following conditions: temperature 180°C, constant pressure in the autoclave (2.5, 6, 11 and 21 bar(a)), stirring speed 950 rpm, concentration of the NiAl catalyst in oil 0.03 wt% (as Ni), 25 g of canola oil. Hydrogen was supplied to a reaction mixture from the bottom by means of a dip tube. The autoclave was loaded with a suspension of the catalyst in oil, the system was evacuated several times and filled with hydrogen in order to remove oxygen. The suspension was then heated under slight vacuum to the required temperature followed by loading the autoclave with hydrogen to the working pressure. The stirring was started and the reaction time was counted from that moment. In order to maintain the constant pressure during hydrogenation, the hydrogen consumed in the course of the reaction was continuously supplied from the reservoir. A decrease of hydrogen pressure in the reservoir was a measure of the hydrogen consumption for hydrogenation of canola oil. After the test, the catalyst was filtered off and a liquid fraction was subjected to analysis. The iodine value (IV) was controlled by means of refractometry. The final IV was determined by means of the titration method using a Wijs reagent [24].

Fatty acid profile analysis

The fatty acid (FA) profiles of hydrogenated samples were analyzed by means of gas chromatography coupled with mass spectrometry using a Shimadzu GC-

MS2010Ultra instrument. The oil samples were subjected to derivatization prior to analysis in order to obtain methyl esters of fatty acids (FAME). A 10 mg sample of hydrogenated canola oil was dissolved in 500 µl *t*-butylmethylether, 250 µm 0.1 % TMSH in MeOH (Fluka) was added and a mixture was vigorously shaken for 45–60 s. The sample was analyzed using the following conditions: BPX column, 120 m × 0.25 mm × 20 µm, isothermal programme 180 °C for 110 min, helium flow 1.0 ml/min, split 100:1. The peaks of particular FAMEs were identified based on mass spectra by comparison with a FAME Mix standard from Restek (37 components). The content of fatty acids was determined by means of the internal normalization, assuming similar response factors of a FID detector for structurally similar FAME compounds.

Results and discussion

Composition and physicochemical properties of NiAlCe precursors and catalysts

The chemical composition of precursors is summarized in Table 1. The results indicate a very good consistence between nominal and actual composition of precursors. The Ni and Ce content in final catalysts after dilution with the hydrogenated protective fat is presented in Table 2. The physicochemical properties of NiAlCe precursors such as specific surface area, pore volume, nickel surface area, dispersion and nickel crystallite size have been determined and compared with the properties of the cerium-free precursor NiAl_0Ce. These results are compiled in Table 3, whereas the results of the pore size distribution analysis in the pore size range of 2–300 nm are demonstrated in Fig. 1.

Table 1 The chemical composition of NiAlCe precursors by means of XRF

Precursor	Theoretical composition (%)	Metal content (wt%)		Oxides content (wt%)		
		Ni	Ce	NiO	CeO_2	Al_2O_3
NiAl_0Ce	NiO 85.0 Al_2O_3 15.0	67.3	–	85.9	–	14.1
NiAl_1Ce	NiO 85.0 CeO_2 5.0 Al_2O_3 10.0	64.9	3.68	82.8	4.50	12.7
NiAl_2Ce	NiO 85.0 CeO_2 7.5 Al_2O_3 7.5	64.4	5.65	82.2	6.94	10.9
NiAl_3Ce	NiO 85.0 CeO_2 10.0 Al_2O_3 5.0	66.4	7.75	84.7	9.52	5.77

Table 2 The chemical composition of NiAlCe catalysts

Catalyst	Ni content (wt%)	Ce content (wt%)
NiAl_0Ce_C	5.64	0
NiAl_1Ce_C	5.55	0.36
NiAl_2Ce_C	5.76	0.56
NiAl_3Ce_C	4.95	0.67

Table 3 Physicochemical properties of NiAlCe precursors

Precursor	Specific surface area, S_{BET} (m^2/g)	Nickel surface area, S_{Ni} (m^2/g_{cat})	Nickel surface area, S_{Ni} (m^2/g_{Ni})	Total pore volume, V_C (cm^3/g)	Mesopore volume, V_{mes} (cm^3/g)	Ni crystallite size, d_{av} (nm)	Dispersion, D (%)
NiAl_0Ce	70	42.6	63.1	0.34	0.17	11.2	9.5
NiAl_1Ce	132	38.0	58.4	0.44	0.22	12.1	8.8
NiAl_2Ce	218	30.9	47.7	0.53	0.26	14.8	7.2
NiAl_3Ce	220	35.4	53.1	0.49	0.30	13.3	8.0

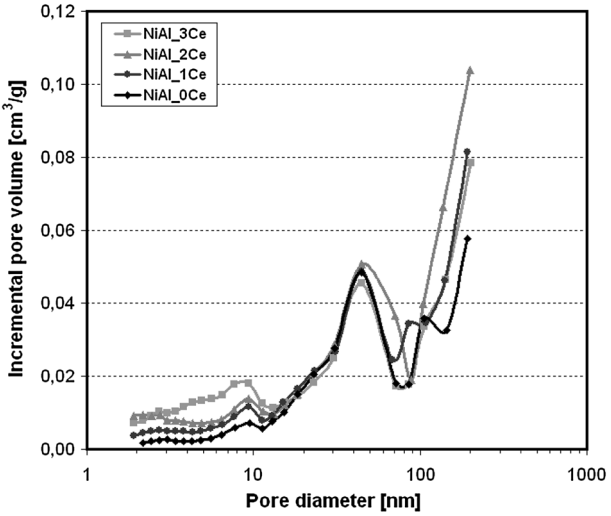

Fig. 1 Pore size distribution of NiAl and NiAlCe precursors

The results indicate that cerium acts as a structural promoter influencing considerably the specific surface area. The threefold increase of the S_{BET} value from 70 to 218 m^2/g was observed between the cerium-free precursor NiAl_0Ce and NiAl_2Ce. A further increase of the cerium content above 5.65 wt% did not result in increase of S_{BET}. The pore distribution analysis in a given range revealed that after

calcination the dominant pores were in the range from 10 to 100 nm. This corresponds to the intermediate structure between meso- and macroporous. The pore volume was found to increase with the increased cerium content up to 5.65 wt% and then it decreased insignificantly in case of NiAl_3Ce. On the other hand, the mesopore volume increased constantly with the increased cerium content from 0.17 to 0.30 cm^3/g. The increase of the specific surface area is a consequence of the increase of mesopore volume.

XRD was used to compare the phase composition of NiAlCe precursors. The diffractograms at room temperature are shown in Fig. 2. The analysis of the position and intensity of diffraction lines revealed in crystallographic composition a phase of nickel–aluminum hydroxycarbonate of the takovite-type, $Ni_6Al_2(OH)_{16}(CO_3)\cdot 4H_2O$ (ICDD 15-87). Upon increasing the cerium content, the crystallinity of that phase was found to decrease as indicated by broader peaks of lower intensity. Similarly to

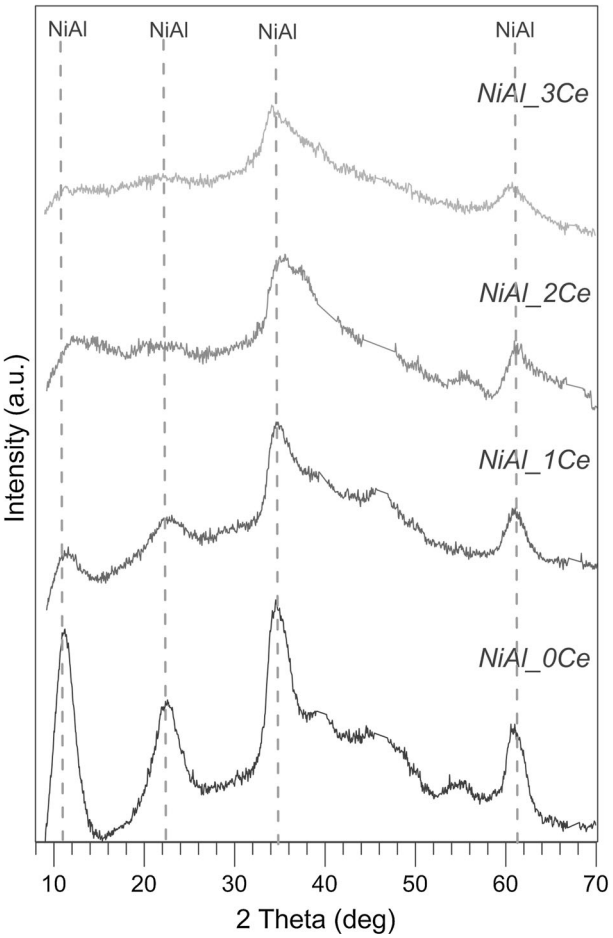

Fig. 2 XRD diffractograms of NiAl and NiAlCe precursors (diffraction lines for a platinum strip are omitted for clarity)

the CuZnAl hydroxycarbonates with a hydrotalcite-like structure, $Ni_6Al_2(OH)_{16}(CO_3)\cdot 4H_2O$ exhibits a layered structure of the LDH type (layered double hydroxide) with interlayer water molecules and carbonate anions [25]. This phase is characterized by peaks with the highest intensity peaks at 2θ angles 11.1° and 22.6° corresponding to (003) and (006) diffraction planes, respectively. In diffractograms of the cerium-promoted NiAlCe precursors no crystalline phases of cerium oxide could be identified. This indicates that the phase of cerium oxide is well dispersed or crystallites are below the XRD detection limit, i.e., ca. 2 nm.

Figs. 3 and 4 present the DTG curves and MS profiles corresponding to signals with $m/z = 18$ (H_2O) and 44 (CO_2) for NiAl_0Ce and NiAl_3Ce precursors. A comparison of the thermal decomposition of both precursors with no cerium and 10 wt% of cerium revealed no significant differences. The thermal decomposition proceeded in two stages up to the temperature of 450 °C. In the first stage up to ca. 225 °C, the evolution of water vapor (moisture and crystallization water) was observed. In the second step proceeding in the range of 230–450 °C, the evolution of water vapor and CO_2 took place as a result of the decomposition of hydroxyl and carbonate groups of nickel–aluminum hydroxycarbonates. This stage was a little bit more intensive in case of the NiAl_3Ce precursor.

The TPR reduction profiles of NiAlCe precursors are shown in Fig. 5. The NiAl_0Ce precursor underwent reduction in a single stage in a wide temperature range from 250 to 600 °C. The maximum reduction rate was achieved at 385 °C. The addition of cerium resulted in a shift of that temperature maximum by ca. 50°C

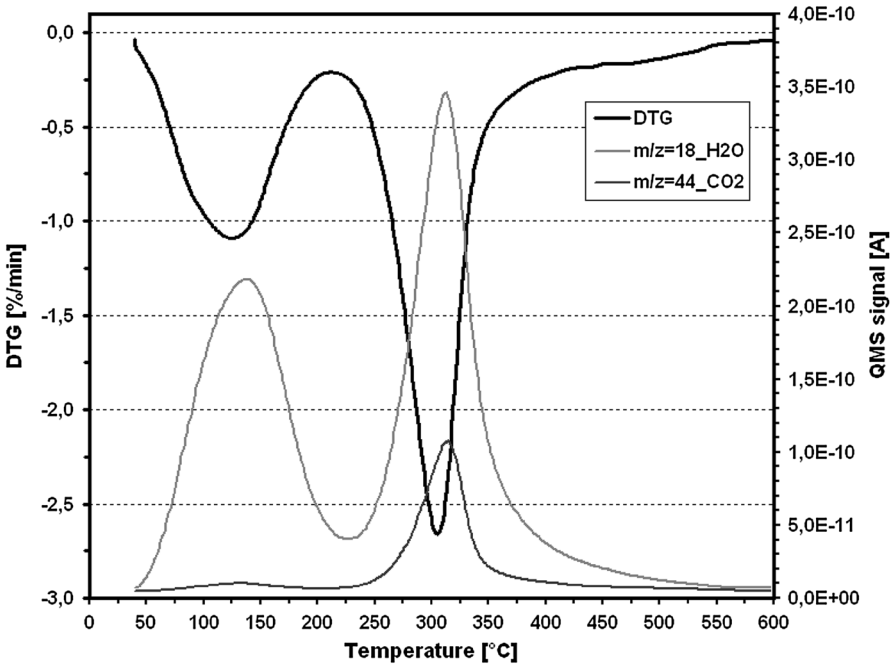

Fig. 3 DTG and S_{QMS} profiles of the NiAl_0Ce precursor

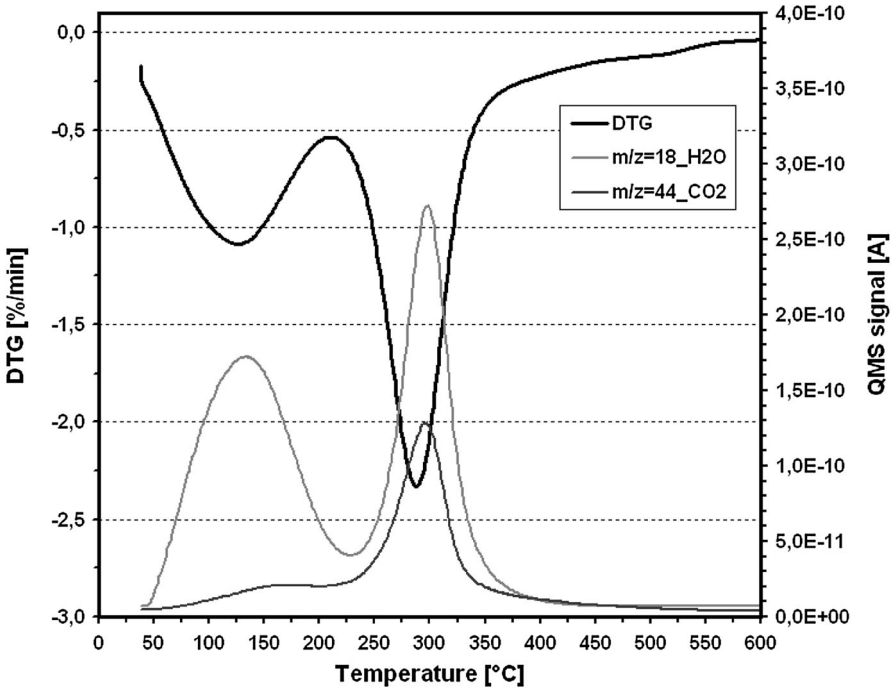

Fig. 4 DTG and S_{QMS} profiles of the NiAl_3Ce precursor

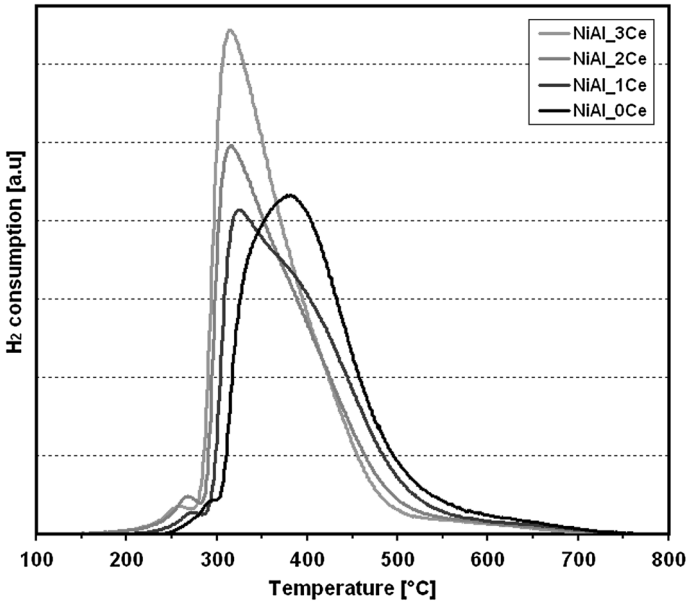

Fig. 5 TPR profiles of the NiAl and NiAlCe samples

towards lower temperatures, independently of the cerium content. The reduction of the cerium-promoted precursors proceeds easier and with the increased cerium content the TPR profiles become more intensive indicating more homogeneous form of reduced NiO.

The changes in phase composition during concurrent thermal decomposition and reduction of precursors were also monitored by means of the HT-HRD technique (Fig. 6). The increase of temperature to 200 °C resulted in a shift of the (003) diffraction line from 11.1° towards higher 2θ angles (100 °C, 12.8°; 200 °C, 13.9°) with a concurrent decrease of the intensity. This observation can be attributed to the removal of interlayer and weakly bound water leading to the formation of the intermediate dehydrated phase [25–27]. However, in contrast to CuZnAl-LDH, for which the intermediate phase was reported to be retained up to 150–200 °C [25], in the case of the takovite-like phase the intermediate phase is retained up to 200–250 °C. In the diffractogram of the NiAl_0Ce precursor at 300 °C, only very broad diffraction lines of a low intensity could be observed indicating a very low crystallinity of components. This observation is further supported by the DTG results showing that above 200 °C co-evolution of H_2O (elimination of the structural hydroxyl groups) and CO_2 (removal of interlayer and structural carbonate groups) occurs leading to the collapse of the ordered layered structure. At 400 °C

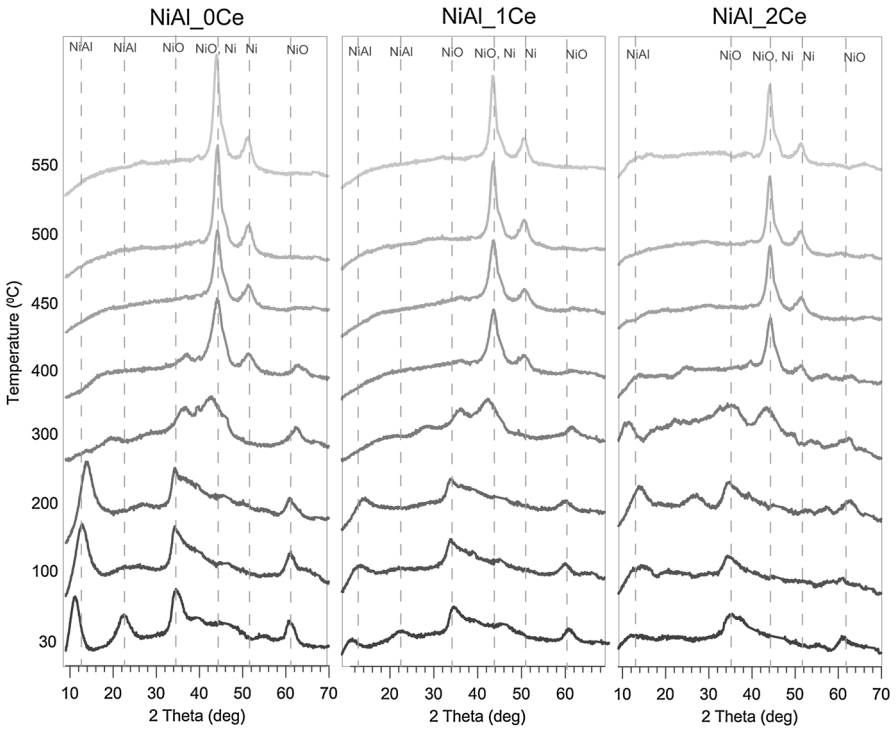

Fig. 6 HT-XRD diffractograms of the NiAl and NiAlCe precursors during thermal decomposition/reduction in 5 % H_2/N_2

NiO and Ni phases were observed indicating crystallization of NiO and its concurrent reduction to Ni. The first measurement at 450 °C revealed still traces of the NiO phase, but after 45 min only the Ni phase was identified indicating a complete NiO reduction.

The nickel surface area was observed to decrease with the incorporation of cerium (from 42.6 for NiAl_0Ce to 30.9 m^2/g_{cat} for NiAl_2Ce). Concerning nickel crystallite size, this parameter was found to increase from 11.2 to 14.8 nm with the increased cerium content, whereas nickel dispersion decreased from 9.5 to 7.2 for NiAl_2Ce.

Catalytic activity of NiAlCe catalysts

The catalytic activity of the NiAlCe catalysts was tested in the hydrogenation reaction of canola oil. The measurements were carried out at the temperature of 180 °C typically used in oil industry and in a wide range of pressures from 2.5 to 21 bar(a). The agitation rate was 950 rpm. It was verified that the agitation rate above 950 rpm had no effect on the hydrogenation rate. This indicates that above the agitation rate of 950 rpm there are no diffusional resistances for a transfer of dissolved hydrogen to the bulk liquid phase and then to the catalyst surface. In all tests, the hydrogenation depth of canola oil samples was on a similar level as indicated by similar changes of the iodine value (IV) measured by means of refractometry ($\Delta IV = 43–47$) and a final IV determined by means of the Wijs method ($IV = 69–72$). Table 4 presents the activity results for cerium-free and cerium-promoted catalysts. The effect of the hydrogen pressure on hydrogenation time for cerium-modified nickel catalysts is summarized in Fig. 7. The nickel content in the reaction suspension was in each test the same and equal to 0.03 wt%. Two approaches for the estimation of the hydrogenation activity were used. In the first one, the activity is expressed by the hydrogen consumption per 1 g of Ni per min (comparable hydrogenation depth of all samples). The second approach is based on the overall apparent reaction constant k_r, according to Plourde et al. [28].

It is well known that the saturation of double bonds follows first-order kinetics with respect to the iodine value drop as shown in Eq. 5:

$$\frac{1}{m}\frac{\mathrm{d}(\mathrm{IV})_\mathrm{t}}{\mathrm{d}t} = -k_r \cdot (\mathrm{IV})_\mathrm{t} \tag{5}$$

The integration of Eq. 5 using the initial conditions that $(IV)_t = (IV)_0$ at $t = 0$ gives:

$$m \cdot k_r = \frac{1}{t} \cdot \ln\left(\frac{\mathrm{IV}_0}{\mathrm{IV}_\mathrm{t}}\right) \tag{6}$$

In line with expectations, a considerable increase of the catalytic activity in canola oil hydrogenation was observed with the increased hydrogen pressure. In case of the cerium-free catalyst, NiAl_0Ce_C consumption of 1000 cm^3 hydrogen by the oil lasted ca. 30 min shorter upon rising up the pressure from 2.5 to 21 bar(a) (39 vs. 7 min). Concerning the cerium effect, several conclusions can be

Table 4 Hydrogenation of canola oil on cerium-modified nickel catalysts

Test	p [bar(a)]	Δp	Time (min)	A [cm^3 H_2/(g Ni min)]	mk_r (min^{-1})	k_r [(kg of oil) (g of Ni)$^{-1}$ min^{-1}]	Change of iodine value ΔIV	IV_{Wijs}
NiAl_0Ce_C								
1	2.5	10.8	39	3350	0.013	0.043	46.2	71.2
2	6.0	10.8	19.3	6770	0.027	0.089	46.2	–
3	11.0	10.9	12	11,000	0.042	0.142	45.8	–
4	21.0	11.0	7	19,050	0.075	0.251	47.0	69.2
NiAl_1Ce_C								
5	2.5	10.8	38	3440	0.013	0.043	44.8	71.6
6	6.0	10.8	18	7260	0.028	0.092	44.8	–
7	11.0	10.9	11	12,000	0.045	0.150	44.7	–
8	21.0	11.0	9	14,815	0.055	0.184	44.8	70.1
NiAl_2Ce_C								
9	2.5	10.8	40	3270	0.013	0.043	46.0	69.5
10	6.0	11.0	20.5	6500	0.024	0.081	44.8	–
11	11.0	10.9	14	9430	0.036	0.119	45.2	–
12	21.0	10.8	11	11,880	0.044	0.147	44.0	69.8
NiAl_3Ce_C								
13	2.5	10.9	56	2360	0.009	0.030	45.7	69.4
14	6.0	10.8	33	3960	0.015	0.051	45.2	–
15	11.0	10.9	16	8250	0.030	0.098	43.2	–
16	21.0	10.8	13	10,050	0.037	0.123	43.7	69.8

drawn from the activity measurements. As can be observed, the addition of cerium clearly inhibited the hydrogenation process, especially at highest cerium content and pressures. Generally, the activity of cerium-promoted catalysts with the cerium content above 0.36 wt% was found to be lower than that of the cerium-free catalyst in the entire pressure range under study [11 bar(a): NiAl_0Ce_C, 11,000 cm^3 H_2/(g Ni min); NiAl_3Ce_C, 8250 cm^3 H_2/(g Ni min)]. The results also reveal that the activity decreases with the increased cerium content [2.5 bar(a): 38 min and 3440 cm^3 H_2/(g Ni min) for NiAl_1Ce_C; 56 min and 2360 cm^3 H_2/(g Ni min) for NiAl_3Ce_C].

Selectivity of NiAlCe catalysts

The results of the selectivity of cerium-promoted nickel–aluminum catalysts in hydrogenation of canola oil are presented in Table 5. These results indicate that the addition of cerium impedes the formation of C18:1 *trans* isomers of fatty acids, both 4-9t and 10-14t ones. This positive effect of cerium was found to increase with the increased cerium content, and was more pronounced at lower pressures. In the

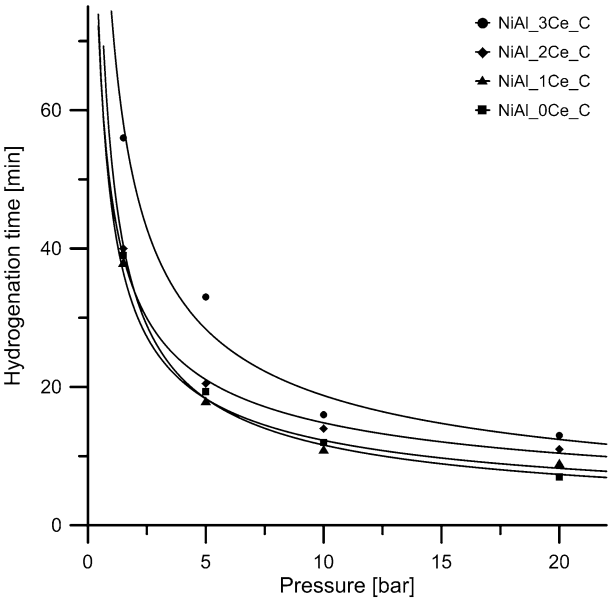

Fig. 7 Effect of the hydrogen pressure on the hydrogenation time of canola oil for cerium-modified nickel catalysts (180° C, 950 rpm, 0.03 wt% of Ni)

hydrogenation reaction under the pressure of 2.5 bar(a), the content of C18:1 *trans* isomers decreased from 36.2 % for the cerium-free catalyst, NiAl_0Ce_C to 27.2 % for the NiAl_3Ce_C catalyst containing 0.67 % of cerium. However, the influence of cerium on C18:1 *trans* isomers was observed to decrease with the increased pressure (21 bar(a); 22.8 % for NiAl_0Ce_C, 18.7 % for NiAl_3Ce_C). Taking into account that an increase of hydrogen pressure has also a substantial effect on the TFA isomer content, both effects (pressure and cerium) resulted in a significant decrease of C18:1 *trans* fraction by ca. 48 % (from 36.2 to 18.7 %). The effect of the suppression of the *cis/trans* isomerization has been recently reported by Stanković et al. in hydrogenation of soybean oil at 160 °C and at 1.6 bar for silver-modified diatomite-supported NiMg catalysts [29].

The addition of cerium results in a lower content of all *trans* isomers, including additionally isomers of linoleic acid, C18:2 *trans,trans/cis,trans/trans,cis*. Interestingly, with the increase of the cerium content, the share of C18:2 *tt/ct/tc* isomers was found to increase slightly (2.5 bar(a); 1.5 % for NiAl_0Ce_C vs. 2.5 % for NiAl_3Ce_C). This effect becomes less pronounced at higher pressures up to 11 bar(a) (2.1 % for NiAl_0Ce_C vs. 2.3 % for NiAl_3Ce_C) and remains at similar level above this pressure. Overall, both effects of cerium and hydrogen pressure leads to the decrease of all TFA isomers from 37.7 to 20.9 %.

An increase of the content of C18:1 *cis* isomers at the expense of *trans* ones, which is observed with the increased pressure, is also accompanied by an increase of the SFA content, mainly stearic acid, C18:0. In case of the cerium-free catalyst upon increasing pressure from 2.5 to 21 bar(a) an increase of the C18:0 fraction in

Table 5 Percent composition of hydrogenated canola oil samples obtained at various pressures on NiAlCe catalysts. All composition values in wt%, average reproducibility ~0.2–0.5 wt%

FA	Refined canola oil	NiAl_0Ce_C				NiAl_1Ce_C				NiAl_2Ce_C				NiAl_3Ce_C			
		p [bar(a)]															
		2.5	6	11	21	2.5	6	11	21	2.5	6	11	21	2.5	6	11	21
C16:0	4.6	4.6	4.7	4.6	4.6	4.5	4.7	4.5	4.6	4.5	4.5	4.6	4.5	4.6	4.6	4.7	4.6
C18:0	1.1	13.1	16.3	16.7	22.0	13.0	15.1	15.8	19.2	13.4	14.1	16.9	18.6	14.9	16.6	16.8	18.1
C18:1 *trans*[a]	0	36.2	30.6	25.1	22.8	32.8	29.8	26.0	18.7	32.4	26.9	24.6	18.8	27.7	26.4	23.7	18.7
C18:1 *cis*[b]	66.0	41.4	42.6	46.1	41.8	44.4	44.5	46.4	47.9	44.3	47.7	46.6	48.6	46.2	45.7	46.9	49.7
C18:2 *cis/cis*	18.9	0.6	1.2	2.4	3.3	0.8	1.4	2.1	3.9	0.8	1.7	2.3	3.8	1.3	1.6	2.5	3.4
C18:2 *tt/ct/tc*	0	1.5	1.8	2.1	2.0	1.7	1.8	2.2	2.1	1.9	2.2	2.0	2.1	2.5	2.3	2.3	2.2
C18:3	7.8	0	0	0.2	0.5	0	0	0.2	0.5	0	0	0.2	0.5	0	0	0.2	0.5
Other[c]	1.6	2.5	2.8	2.9	2.9	2.7	2.7	2.8	3.0	2.7	2.8	2.9	3.1	2.8	2.8	2.9	2.8
ΣTFA	0	37.7	32.4	27.2	24.8	34.5	31.6	28.2	20.8	34.3	29.1	26.6	20.9	30.2	28.7	26.0	20.9

[a] C18:1 *trans* includes three chromatographically separable group of isomers: C18:1 4t-9t, C18:1 10t-14t and C18:1 16t

[b] C18:1 *cis* includes two chromatographically separable group of isomers: C18:1 9c, and C18:1 10-15c

[c] Other FA includes above all C20:0, C20:1, C22:0, C22:1

the hydrogenated canola oil samples from 13.1 to 22.0 % was observed. Concerning the cerium effect, the addition of cerium does not significantly influence the amount of the C18:0 fraction up to pressures of 11 bar(a). However, cerium has a beneficial influence on the C18:0 amount at the highest pressure. Compared to the canola oil hydrogenation on NiAl_0Ce_C, hydrogenation on NiAl_3Ce_C resulted in the decrease of the C18:0 fraction from 22.0 to 18.1 %. The chromatographic analyses of the FA profiles in hydrogenated samples indicate that the content of linoleic acid also increases with the increased pressure [NiAl_0Ce_C; 0.6 % at 2.5 bar(a) vs. 3.3 % at 21 bar(a)]. Similarly, cerium addition influences the content of linoleic acid but only at lowest pressure (2.5 bar(a); 0.6 % for NiAl_0Ce_C vs. 1.3 % for NiAl_3Ce_C). Furthermore, an increase of pressure was found to affect the content of linolenic acid, C18:3. Some deterioration of the linolenic selectivity was observed at elevated hydrogen pressures as evidenced by an increase of the C18:3 content from 0.2 at 11 bar(a) to 0.5 wt% at 21 bar(a). Similar observations were reported by List et al. for the supported nickel catalyst in the soybean oil hydrogenation at various pressures [30].

There is no reasonable mechanistic explanation at that stage of investigations for better *cis/trans* selectivity of cerium-promoted nickel–aluminum catalysts. The reason for hampering by cerium the *cis/trans* isomerization reaction of C18:1 fatty acids is entirely speculative and the effect of cerium should be presumably rationalized on the basis of the Horiuti–Polanyi mechanism [31]. This mechanism assumes that hydrogenation proceeds through a partially hydrogenated transition state, in which only one hydrogen atom is bound. Particular steps of the Horiuti–Polanyi mechanism are generally reversible so two scenarios may happen at the stage of partial hydrogenation: either the second hydrogen is bound (saturation) or the already bound hydrogen is given back to the metal. The second case may lead to *cis/trans* isomerization. If a cleaved hydrogen atom is the same as the one that was bound, an originally adsorbed compound is reconstituted. Cleavage of the second hydrogen atom on the same carbon atom results in *cis/trans* isomerization and cerium may presumably impede such cleavage. The limited formation of C18:1 *trans* on cerium-promoted nickel–aluminum catalysts can be presumably rationalized in terms of the modification of electronic properties by dopant and the presence of geometric effects as it was also postulated by Stanković et al. for silver-modified diatomite-supported NiMg catalysts [29].

Besides the FA composition of canola oil samples hydrogenated to the iodine value of ca. 70, changes of FA profiles in the course of hydrogenation were also investigated. The FA profiles for two catalysts, NiAl_0Ce_C and NiAl_3Ce_C obtained at pressure of 1.5 bar(a) are presented in Figs. 8 and 9. The results clearly show that significantly less C18:1 *trans* fraction is generated during hydrogenation of canola oil on cerium-promoted nickel-catalyst. This effect is reflected in a slope of the M-*trans* curve that is much steeper in case of the cerium-free catalyst. After 60 min of hydrogenation at 180°C and under 1.5 bar(a), the content of C18:1 *trans* isomers in the hydrogenated samples was ca. 12 % lower in case of the NiAl_3Ce_C catalyst. Moreover, the intersection point of C18:1 *cis* and C18:1 *trans* curves lies at ca. 60 min in case of the NiAl_0Ce_C catalyst and at ca. 110 min for the NiAl_3Ce_C one. This indicates a slower drop of the C18:1 *cis*

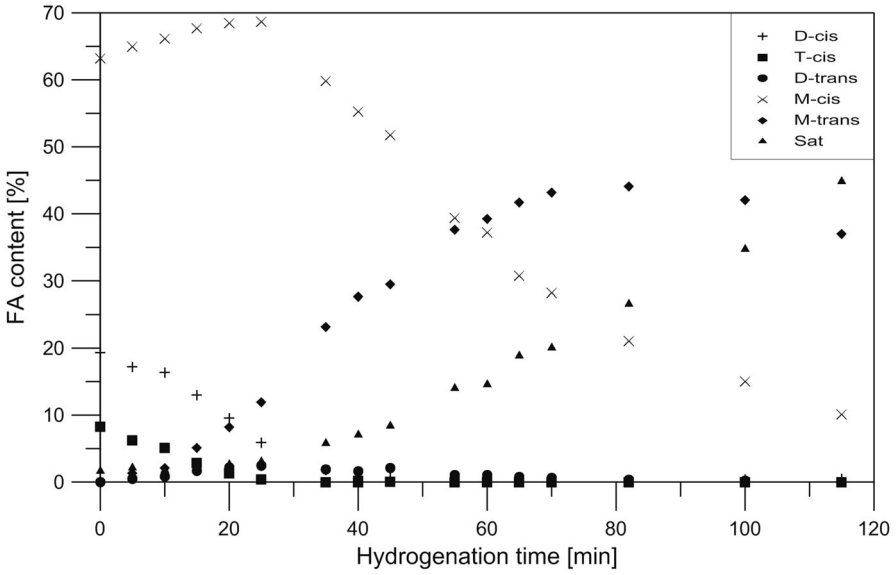

Fig. 8 Changes of the FA composition during hydrogenation of canola oil on NiAl_0Ce_C, 1.5 bar(a), 180 °C, 950 rpm, 0.03 wt% of Ni (T—C18:3, D—C18:2, M—C18:1, Sat—C18:0)

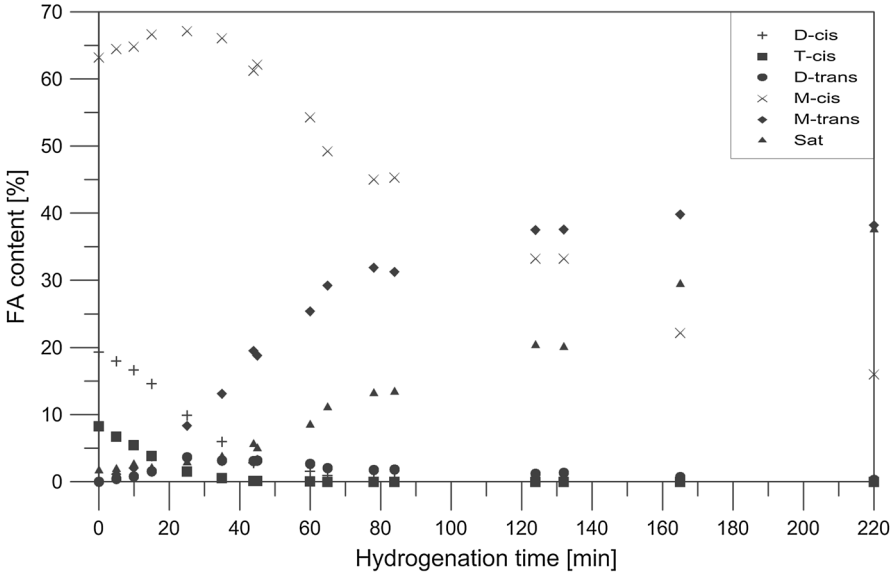

Fig. 9 Changes of the FA composition during hydrogenation of canola oil on NiAl_3Ce_C, 1.5 bar(a), 180° C, 950 rpm, 0.03 wt% of Ni (T—C18:3, D—C18:2, M—C18:1, Sat—C18:0)

fraction that is also accompanied by a slower increase of the C18:0 fraction. Concerning the C18:2 fraction, addition of cerium impedes the hydrogenation of polyunsaturated fatty acids, hydrogenation process proceeds slower in case of the

NiAl_3Ce_C catalyst as indicated by the content of C18:2 *cis* fraction after 40 min of hydrogenation (ca. 5 %).

Conclusions

The incorporation of cerium into co-precipitated nickel–aluminum precursors results in a significant increase of the specific surface area and mesopore volume. However, for these nickel-rich precursors, no effect on active surface area is observed. Moreover, the addition of cerium facilitates the reduction process of the precursor compared to the cerium-free one. The reduction of the cerium-promoted precursors proceeds easier and with the increased cerium content the TPR profiles become more intensive indicating more homogeneous form of reduced NiO. The cerium-promoted nickel–aluminum catalysts exhibit a superior selectivity in hydrogenation of canola oil, yet at the expense of lower activity. The addition of cerium inhibits the hydrogenation process, especially at high pressures and high cerium loading. Nevertheless, upon addition of a relatively low amount of cerium (0.67 wt%), the content of the C18:1 *trans* fraction decreased by ca. 35 %. Together with the synergistic effect of hydrogen pressure a significant decrease of C18:1 *trans* fraction by ca. 48 % could be achieved. Furthermore, compared to the cerium-free catalyst, the addition of cerium resulted in a slower drop of the C18:1 *cis* fraction and a slower increase of the C18:0 fraction. The addition of cerium slightly impedes the hydrogenation of polyunsaturated fatty acids, especially C18:2 fraction.

The results of our studies clearly indicate that utilization of cerium-promoted nickel–aluminum catalysts may lead to a remarkable decrease of the content of deleterious TFA isomers. Further studies seem to be necessary in order to elucidate the role of cerium in the hydrogenation mechanism.

Acknowledgments The authors thank Mr. J. Ostrowski, M.Sc. for his ICP-OES analysis.

References

1. Moulton KJ, Beal RE, Griffin EL Jr (1971) J Am Oil Chem Soc 48:499–502
2. Fernández MB, Tonetto GM, Crapiste GH, Damiani DE (2007) J Food Eng 82:199–208
3. Beers A, Ariaansz R, Okonek D (2008) In: Dijkstra AJ, Hamilton RJ, Hamm W (eds) Trans fatty acids. Blackwell Publishing, Oxford
4. Ascherio A, Katan MB, Zock PL, Stampfer MJ, Willett WC (1999) New Engl J Med 340:1994–1998
5. Hu FB, Stampfer MJ, Manson JE, Rimm E, Colditz GA, Rosner BA, Hennekens CH, Willet WC (1997) New Engl J Med 337:1491–1499
6. Katan MB, Zock PL, Mensink RP (1995) Annu Rev Nutr 15:473–493
7. Mensink RP, Zock PL, Katan MB, Hornstra G (1992) J Lipid Res 33:1493–1501

8. Mozaffarian D, Katan MB, Ascherio A, Stampfer MJ, Willet WC (2006) New Engl J Med 354:1601–1613
9. Philippaerts A, Jacobs PA, Sels BF (2013) Angew Chem Int Ed 52:5220–5226
10. Pandarus V, Gingras G, Beland F, Ciriminna R, Pagliaro M (2012) Org Process Res Dev 16:1307–1311
11. Philippaerts A, Paulussen S, Breesch A, Turner S, Lebedev OI, Van Tendeloo G, Sels B, Jacobs P (2011) Angew Chem Int Ed 50:3947–3949
12. Philippaerts A, Breesch A, De Cremer G, Kayaert P, Hofkens J, Van den Mooter G, Jacobs P, Sels B (2011) J Am Oil Chem Soc 88:2023–2034
13. Jang ES, Jung MY, Min DB (2005) Compr Rev Food Sci Food Saf 1:22–30
14. Menaa F, Menaa A, Treton J, Menaa B (2013) J Food Sci 78:377–386
15. Leclercq E, Rives A, Payen E, Hubaut R (1998) Appl Catal A 168:279–288
16. Vile G, Dahler P, Vecchietti J, Baltanas M, Collins S, Calatayud M, Bonivardi A, Perez-Ramirez J (2015) J Catal 324:69–78
17. Vile G, Bridier B, Wichert J, Perez-Ramirez J (2012) Angew Chem Int Ed 51:8620–8623
18. Wang P, Zhang J, Bai Y, Xiao H, Tian S, Xie H, Yang G, Tsubaki N, Han Y, Tan Y (2016) Appl Catal A 514:14–23
19. Toemen S, Abu Bakar WAW, Ali R (2014) Bull Korean Chem Soc 35:2349–2356
20. Znak L, Stołecki K, Zielinski J (2005) Catal Today 101:65–71
21. Li C, Domen K, Maruya K, Onishi T (1993) J Catal 141:540–547
22. Toyoda T, Nishihara Y, Qian EW (2014) Fuel Process Technol 125:86–93
23. Alouche A, Hubaut R, Bonnelle JP, Davies P, Lambert D (1993) In: Barbier J, Barrault J, Bouchoule C, Duprez D, Montassier C, Guisnet M, Pérot G (eds) Heterogeneous catalysis and fine chemicals III. Elsevier Science, p. 235
24. Method PN-EN ISO 3961. http://sklep.pkn.pl/pn-en-iso-3961-2013-10e.html
25. Kowalik P, Konkol M, Kondracka M, Próchniak W, Bicki R, Wiercioch P (2013) Appl Catal A 464–465:339–347
26. Pérez-Ramírez J, Abelló S, van der Pers NM (2007) Chem Eur J 13:870–878
27. Mokhtar M, Inayat A, Ofili J, Schwieger W (2010) Appl Clay Sci 50:176–181
28. Plourde M, Belkacemi K, Arul J (2004) Ind Eng Chem Res 43:2382–2390
29. Stanković M, Čupić Ž, Gabrovska M, Banković P, Nikolova D, Jovanović D (2015) React Kinet Mech Cat 115:105–127
30. List GR, Neff WE, Holliday RL, King JW, Holser R (2000) J Am Oil Chem Soc 77:311–314
31. Horiuti I, Polanyi M (1934) Trans Faraday Soc 30:1164